Composites of Double-Walled Carbon Nanotubes with bis-Quaterthiophene-Fluorenone Conjugated Oligomer: Spectroelectrochemical and Photovoltaic Properties

Lionel Picard,[†] Frédéric Lincker,[†] Yann Kervella,[†] Malgorzata Zagorska,[‡] Rémi DeBettignies,[§] Alain Peigney,[∥] Emmanuel Flahaut,[∥] Guy Louarn,[⊥] Serge Lefrant,[⊥] Renaud Demadrille,*[,†] and Adam Pron.*[,†]

Laboratoire d'Electronique Moléculaire Organique et Hybride, CEA-INAC-SPrAM, 17, Rue des Martyrs, F-38054 Grenoble, France, Faculty of Chemistry, Warsaw University of Technology, 00664, Warszawa Noakowskiego 3, Poland, Laboratoire Composants Solaires, INES-RDI DRT/LITEN/DTS/LCS, Savoie Technolac BP 332 - 50 avenue du lac Léman, F-73377 Le Bourget du Lac, France, Institut Carnot CIRIMAT, UMR CNRS/UPS/INPT No. 5085, Université Paul Sabatier, F-31062 Toulouse Cedex 9, France, and Institut des Matériaux Jean Rouxel, (IMN), Université de Nantes - CNRS, 2 Rue de la Houssinière, B.P. 32229, F-44322, Nantes Cedex 3, France

A new composite consisting of a semiconducting oligomer, namely 2,7-bis-(3,3‴-didodecyl-[2,2′,5′,2″;5″,2‴]quaterthiophen-5-yl)-fluoren-9-one (QTF12), and double wall carbon nanotubes (DWCNT) has been prepared in view of its application as an active component in bulk heterojunction photovoltaic cells. Raman spectroelectrochemical investigations show that the onset of the oxidative doping of QTF12 in the presence of DWCNT occurs at $E = 0.475$ V vs Ag/Ag^+, that is, by 50 mV lower than in the case of pure QTF12. This effect was independently confirmed by UV−vis-NIR spectroelectrochemistry. The lowering of the oxidative doping potential, detected by spectroelectrochemistry, can be taken as a spectroscopic evidence of oligomer-nanotube interactions which result in raising, by 0.05 eV, the HOMO level of these QTF12 molecules which are at the interface with DWCNT. Bulk heterojunction test photovoltaic cells consisting of a ternary system (QTF12-DWCNT, PCBM) show the open circuit voltage (V_{oc}) = 0.53 V and the power conversion efficiency of 0.43%.

Introduction

π-conjugated oligomers and polymers are interesting electroactive systems whose electronic, magnetic, and optical properties can precisely be tuned not only by appropriate molecular design but also by modifying their oxidation or protonation states via so-called doping reactions.[1] In both semiconducting (undoped) or conducting (doped) states, they can form molecular composites with other electroactive components of different nature, for example, with carbon nanotubes (CNT). The combination of the peculiar properties of CNT with those of polymers makes such composites potential candidates for a large variety of applications, such as data storage media, supercapacitors, photovoltaic cells, and photodiodes,[2] optical limiting devices and organic light-emitting diodes.[3] In the particular case of photovoltaic applications, which have been developed in recent years, conjugated polymers-CNT composites can serve as components of photoactive materials to generate electricity from light or as highly conductive transparent electrodes.[3]

π-conjugated polymers are known to strongly interact with the carbon nanotube surface through π-stacking interactions to form supramolecular adducts.[4] Such noncovalent functionalization of carbon nanotubes with planar aromatic macromolecules was found to be of a significant interest since it allows nanotube modification without the introduction of defects[4f−i] and at the same time it facilitates the molecular mixing of both composite components.[5] A large majority of the reports, concerning the preparation and the characterization of composites of organic semiconductors or conductors with CNT, focuses on processable polymeric systems such as polythiophene or polyfluorene derivatives and single wall CNT.[4a,c] Much less research work has been carried out on oligomer[4j] or polymer composites with double wall CNT.[5] Similarly, reports on the use of conjugated oligomers as components of photovoltaic cells are scarce.[6,7] This is surprising, since due to their regiochemically well-defined structure and strict monodispersity oligomers exhibit several features that make them attractive candidates for the application as active layers in optoelectronic devices. Monodispersity is here of a crucial importance since polydispersity of π-conjugated polymers is one of the most important factors limiting their electrical transport properties in electronic and optoelectronic devices.[8] Our interest in fluorenone-based well-defined oligomers relies on their capability of serving as efficient donor components in the active layer of bulk-heterojunction solar cells.[7,9] Moreover, it has been shown that their fluorenone units strongly interact with graphite surface.[10] By analogy, strong noncovalent interactions with the carbon nanotubes surface are expected for fluorenone based molecules which should facilitate the processing of molecular composites.

For detailed investigations we have selected a very promising composite consisting of (2,7-bis-(3,3‴-didodecyl-[2,2′;5′,2″;5″,2‴] quaterthiophen-5-yl)-fluoren-9-one, abbreviated as QTF12, and double wall CNT. In particular, we have focused on morphological studies of such composites and on the investigation of

* To whom correspondence should be addressed.
[†] CEA-INAC-SPrAM.
[‡] Warsaw University of Technology.
[§] INES-RDI DRT/LITEN/DTS/LCS.
[∥] UMR CNRS/UPS/INPT No. 5085.
[⊥] Université de Nantes - CNRS.

10.1021/jp906112p

the effect of the DWCNT presence on the redox properties of QTF12 that are governed by the positions of its highest occupied molecular orbital (HOMO) and lowest unoccupied molecular orbital (LUMO) levels with respect to the vacuum level. To accomplish this goal, we have selected UV−vis-NIR and Raman spectroelectrochemistry since both methods are very sensitive toward the redox state of a given conjugated molecule and, if used in the quasi-static mode, enable the determination of the onset of the oxidation or reduction process with very high accuracy. We also explore the effect of the presence of DWCNT on the basic parameters of the solar cells consisting of a three component bulk heterojunction, QTF12/PCBM/DWCNT. The combined studies show that even a very small admixture of DWCNT modifies the electrochemical response of the oligomer and consistently changes the parameters of the fabricated solar cells.

Experimental Section

Chemicals. All commercially available reagents were used without further purification. Solvents were dried and distilled prior to use. All reactions were carried out in standard glassware under inert argon atmosphere. Merck silica gel 60 (0.063−0.200 mm) was used for column chromatography. Solvent evaporation was done at water pressure and samples were further dried in vacuo at 10^{-2} Torr.

Characterization Methods. All synthesized products were identified by ^{1}H and ^{13}C NMR spectroscopy, as well as by elemental analysis. NMR spectra were recorded in chloroform-*d*, containing tetramethylsilane as internal standard, on a Bruker AC200 spectrometer. Elemental analyses (C and H) were carried out by the Analytical Service of the CNRS (Vernaison, France). Ultraviolet−visible (UV−vis) absorption spectra were recorded on a HP 8452A spectrometer (wavelength range 190−820 nm) or on a Varian-Cary 5000 spectrometer in the case of spectroelectrochemical investigations. Raman spectra were recorded either on a (Jobin−Yvon LabRAM HR 800 spectrometer (λ_{exc} = 632 nm) or in Raman spectroelectrochemical studies on a Bruker RFS100 FT-Raman spectrometer (λ_{exc} = 1064 nm).

Synthesis. (3,3‴-Didodecyl-[2,2′5′,2″;5″,2‴]quaterthiophen-5-yl)-trimethyltin was prepared according the procedure described in Supporting Information, starting from 3,3‴-didodecyl-[2,2′5′,2″;5″,2‴]quaterthiophene abbreviated as QT12. The crude compound was titrated by 1H NMR spectroscopy at 90% and used directly for coupling reactions. 2,7-Bis-(3,3‴-didodecyl-[2,2′,5′,2″;5″,2‴]quaterthiophen-5-yl)-fluoren-9-one (QTF12) was prepared according to the procedure described in ref 7. QTF12 was obtained as a deep red waxy product. The spectroscopic characterizations of the molecules can be found in the Supporting Information files.

Preparation of Composites. The following three types of solutions for the samples processing were prepared: (i) solution of QTF12 in chlorobenzene with a concentration of 10 $mg \cdot mL^{-1}$; (ii) solution of QTF12 + 0.1%$_{w/w}$ DWCNT, prepared by dissolving 10 mg of QTF12 in 1 mL of a 10 $\mu g \cdot mL^{-1}$ dispersion of DWCNT in chlorobenzene; and (iii) solution of QTF12 + 1%$_{w/w}$ DWCNT, prepared by dissolving 10 mg of QTF12 in 250 μL of a 0.4 $mg \cdot mL^{-1}$ dispersion of DWCNT in chlorobenzene and subsequently diluting it with 750 μL of pure chlorobenzene. Before coating, the last solution was sonicated for 30 min using a VWR USC300D ultrasonic bath for a maximum disintegration of CNT bundles. The composites were obtained by spin coating from the previously described solutions onto ITO substrates using a SET TP6000 device under a laminar flow controlled by miniflux ESI FRANCE. Solutions (100 μL) were used to coat the whole surface of the substrates (0.5 × 0.5 in.). The coating program is divided in three parts, 20 s at 500 rpm to spread the solution on the entire substrate, 40 s at 1500 rpm to coat the solution, and finally 60 s at 2000 rpm with an acceleration of 200 rpm^2 to dry the layer.

Atomic Force Microscopy. AFM topological and phase images were obtained in intermittent mode using a Nanosurf Mobile S device. The type of cantilever used is NCLR 50 POINTPROBE-silicon SPM sensor. Dimensions are *L*/*W*/*T* of 225/38/7 μm. The resonance frequency is close to 190 kHz and the force constant is 48 N/m. Images were processed using WSXM software developed and distributed by Nanotec Electronica S.L.[11]

Electrochemical and Spectroelectrochemical Investigations. Cyclic voltammetry experiments were performed in an argon glovebox, using a one-compartment electrolytic cell with a platinum disk working electrode (7 mm^2 surface area), a platinum counter electrode, and an Ag/0.1 $mol \cdot L^{-1}$ $AgNO_3$ reference electrode. All spectroelectrochemical and electrochemical experiments were carried out in the same electrolyte consisting of 0.1 M Bu_4NBF_4 solution in acetonitrile. For UV−vis-NIR and Raman spectroelectrochemical investigations, the composites were deposited on an ITO (indium−tin oxide) transparent electrode and on a platinum electrode, respectively. The measurements were carried out in a one compartment cell with a platinum counter electrode and an Ag/0.1 $mol \cdot L^{-1}$ $AgNO_3$ reference electrode. The reference electrode was calibrated versus ferrocene (Fc) couple measured in the same solution.

Photovoltaic Cells Fabrication. Bulk-heterojunction solar cells were fabricated on a glass substrate covered by a transparent conductive oxide, ITO, according to the procedure and layout described in refs 9 and 12. The ITO was covered with a 40 nm thick interfacial PEDOT/PSS layer (Baytron-P) onto which the active layer was spin-coated from chlorobenzene solutions containing the QTF12/DWCNT/PCBM mixture. The thickness of the active layer was 90 nm (± 10 nm). Finally, a 0.8 nm thick layer of LiF was evaporated on top of the active layer and covered by the aluminum electrode (100 nm). The active surface of the devices was 0.28 cm^2. Current−voltage characteristics of the solar cells, illuminated through the ITO, were measured in inert atmosphere via a computer controlled Keithley1 SMU 2400 unit using 100 $mW \cdot cm^{-2}$, AM 1.5 simulated white light generated by a Steuernagel Solar Constant 575 simulator. These simulated conditions are consistent with most published work to date. A monocrystalline silicon solar cell, calibrated at the Fraunhofer Institut Solare Energiesysteme (Freiburg, Germany), was used as a reference cell to confirm stabilization of the 100$mW \cdot cm^{-2}$ illumination. The used apparatus was a standard system that is widely used and gives mismatch factors of around 25% in the 300−1100 nm range. The mismatch factors were obtained by comparison of simulated light with outdoor tests. The temperature of the polymer heterojunction, measured using a thermocouple (Pt100) mounted on the ITO substrate, reached 31 °C during the first *I*−*V* characterization.

Results and Discussion

Nanotubes Preparation. The double-walled carbon nanotubes (DWCNT) that have been used in this study for the fabrication of composites were synthesized by a catalytic chemical vapor deposition (CCVD) method that was reported elsewhere.[13] A $Mg_{0.99}(Co_{0.75}Mo_{0.25})_{0.01}O$ powder was used as a

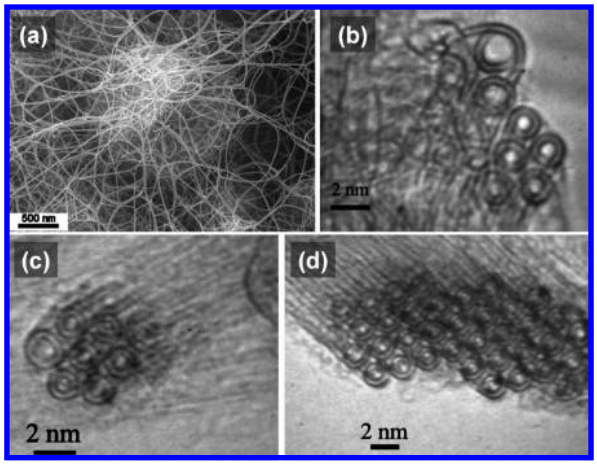

Figure 1. (a) SEM image of the DWCNT-Co/Mo-MgO nanocomposite powder showing the large quantity of CNTs, individual or gathered in bundles, covering the grains of the catalytic material. (b−d) HRTEM images of bundles composed of a few DWCNT, 1.4−2 nm in diameter organized in a triangular network (b,c) or composed of hundreds of DWCNT, 1.2−1.4 nm in diameter (d).

catalytic material and submitted to a thermal treatment at a maximum temperature of 1000 °C in a H_2-CH_4 atmosphere (18 mol % CH_4,), producing a CNT-Co/Mo-MgO nanocomposite powder. This powder then was treated with a 37% HCl aqueous solution in order to dissolve MgO and most of the metal catalyst without damaging the DWCNT.[14] The DWCNT suspension was then filtered and washed with deionized water until neutral pH was measured and then subsequently washed with ethanol. Finally, the sample was dried overnight at 80 °C in air (see Figure 1).

Statistical studies of HRTEM images of individual CNT have shown that most of them (ca. 80%) are double-walled, typically 1−3 nm in diameter, with the other being SWCNT (15%) or triple-walled CNT (5%). They are either individual or gathered in small diameter bundles (10−30 nm), which can be up to ca. 100 μm in length. The carbon content (88.4 ± 0.2 wt % corresponding to ca. 97 mol %) was determined by flash combustion. Additional information concerning the size and the quality of the DWCNT obtained can be extracted from their Raman spectra (Figure 2). In addition, Raman scattering has been fruitfully used in the past to determine the electronic nature of the tubes if one uses the so-called, well-known Kataura plot.[15] Before detailed discussion of the spectrum presented in Figure 2, it is important to note that by Raman spectroscopy, only nanotubes being in resonance with the applied excitation line are detected. In other words, by using only one excitation line, it is impossible to detect all nanotubes present in the sample. In our case, the red excitation line (λ_{exc} = 632 nm) is in resonance with metallic nanotubes as evidenced by the characteristic asymmetric profile of their G band (1576 cm^{-1}) dominating the spectrum.[16] This band is composed of components named G^- and G^+ and its shape was first interpreted as a strong electron−phonon interaction with a continuum of states, characteristic of the metallic nature of the tubes. This gives rise to the so-called Breit−Wigner−Fano (BWF) profile, but recent calculations[17] have also demonstrated that the G^- component is strongly dependent on the tube diameters and therefore can also lead to this asymmetric profile that, in any case, characterizes metallic tubes. The disorder (D) band (1320 cm^{-1}) originates from the presence of nanotube defects such as undesirable sp^3 carbon including disordered carbon, CNT-wall defects, and nanocapsules. Thus, the I_D/I_G ratio can be taken as a measure of the nanotubes quality. In the spectrum presented in Figure 2, this ratio is 6.5%; in spectra recorded from different areas of the sample, it varies from 5 to 11% with the mean value equal to 8.2%. It can be therefore concluded that the prepared batch of DWCNT is relatively homogeneous and the nanotubes contain only a reasonable amount of defects. From the position of the radial breathing mode (RBM) at low wave numbers (usually between 120 to 350 cm^{-1}), it is possible to estimate the DWCNT diameter. Several formulas have been used, such as that proposed by Alvarez et al.[18] used for nanotubes arranged in bundles (ω_{RBM} is the radial breathing mode frequency and d the diameter of the nanotubes)

$$\omega_{RBM}\,(cm^{-1}) = 6.5 + 232/d\,(nm) \qquad (1)$$

The calculations based on the spectrum presented in Figure 2 lead to nanotubes' diameters ranging from 1.09 to 1.96

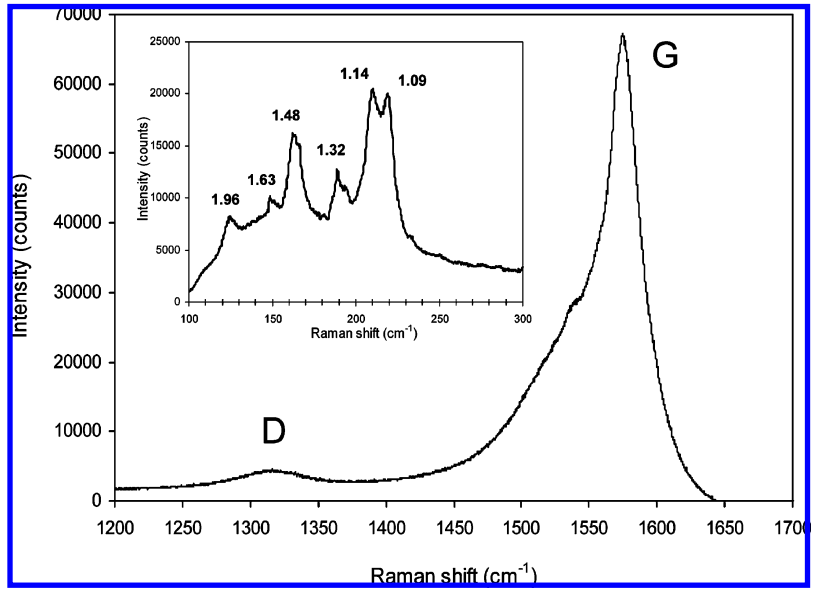

Figure 2. Representative Raman spectrum of DWCNT used for the fabrication of composites with QTF12 (λ_{exc}= 632.82 nm).

SCHEME 1: Chemical Structure of QTF12

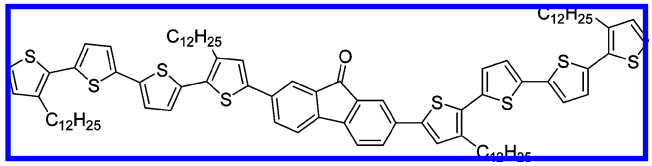

nm. Similar calculations based on the RBM modes recorded for other areas of the sample have shown that most CNT have diameter values ranging between 0.69 and 1.99 nm. Let us mention that in the particular case of DWNT, the RBM bands are observed in two sets; one is reflecting the outer tubes (lower wavenumbers) while the other is associated to inner tubes (higher wavenumbers) (see for, example, ref 19). It should be added that, similarly to SWCNT, the observed peak intensities do not reflect the real amount of CNT of a given diameter because of the resonance effect that amplifies the Raman signal from those CNT that are only in resonance with $\lambda_{exc} = 632$ nm. The use of the infrared excitation line ($\lambda_{exc} = 1064$ nm) leads to a different Raman spectrum of the DWNT studied. In particular, the Lorentzian shape of the G band, combined with the position of the RBM mode, seems to indicate that in this case; the semiconducting nanotubes of lower diameter are in resonance (not shown). In summary, the Raman data show the presence of both metallic and semiconducting nanotubes of diameters varying from 0.7 to 2 nm. This is in good agreement with HRTEM observations indicating the diameter distribution from 0.7 to 3.0 nm, taking into account that nanotubes of $d > 2.0$ nm are difficult to be detected by Raman spectroscopy.

Oligomer Synthesis. QTF12 derivatives (see Scheme 1) was prepared using a synthetic route involving the Stille cross-coupling reaction between 2,7-dibromofluoren-9-one and stanylated 3,3‴-didodecyl-[2,2′;5′, 2″;5″,2‴]-quaterthiophene (QT12).[7] The quaterthiophene segment being synthesized following the procedure reported by Herrema et al.[20] was stannylated by reaction with one equivalent of BuLi followed by the quenching of the corresponding lithiated species with trimethyltin chloride. The four dodecyl side chains of the final molecule ensure its good solubility in classical solvents, often used for the fabrication of organic solar cells, such as chloroform, toluene, cholorobenzene, and orthodichlorobenzene up to 20 mg/mL. The presence of the dodecyl chains also improves the ability of QTF12 to form homogeneous thin films.

Composites Preparation. The composites were obtained by spin coating chlorobenzene solution containing QTF12 and various amount of DWCNT onto ITO substrates. It was found that QTF12 in the presence of DWCNT form a homogeneous and stable (for weeks) solution in chlorobenzene. This may indicate that the fluorenone based molecules are efficiently adsorbed on the nanotube surface, and that the π-stacking interaction between the molecule and the nanotube surface is strong enough to prevent aggregation of nanotubes into larger bundles. In this study, only low concentrations of DWCNT in chlorobenzene were tested, leading to composites with 0.1 and 1 wt % DWCNT content. In the subsequent text they are termed QTF12-0.1%DWCNT and QTF12-1.0%DWCNT. Taking into account a high aspect ratio of DWCNT, a low percolation threshold is expected in such composites.

Composites Morphology. The surface morphology of the QTF12-0.1%DWCNT and QTF12-1.0%DWCNT composites was studied in AFM intermittent mode (topography and phase contrast) as presented for the higher concentrated composite in Figure 3.

These images show, as expected, the presence of two different materials in the composite, the oligomer matrix appears dark whereas the DWCNT appears whiter. On the topographical image, the DWCNT bundles possibly embedded in the QTF12 matrix are over the mean plane of the composites that let them appearing whiter. The different chemical composition of the two materials lead to a different dissipation of the cantilever energy when interacting with the surface. This induces a contrast in the phase image. The dissipation of the cantilever energy is higher in the smoothest material, QTF12, letting it appearing darker.

These large images confirm that a good distribution of the DWCNT bundles is achieved within the film and prove also that a low concentration (ca. 1% in weight) is sufficient to reach the percolation point of the DWCNT. Avoiding percolation of DWCNT is crucial for the use of the composites for photovoltaic applications since metallic tubes are present in the sample. With 0.1% of DWCNT, no percolation exists, for this reason we decided to use this composite for the fabrication of solar cells (vide infra). Higher magnification of the sample (images not shown here), confirm also that the QTF12 phase is rather well-organized between the tubes and forms small fibers like aggregates.

UV−vis-NIR Spectroelectrochemistry. Important parameters, which facilitate the prediction of the suitability of a given oligomer (polymer) for the application in photovoltaic

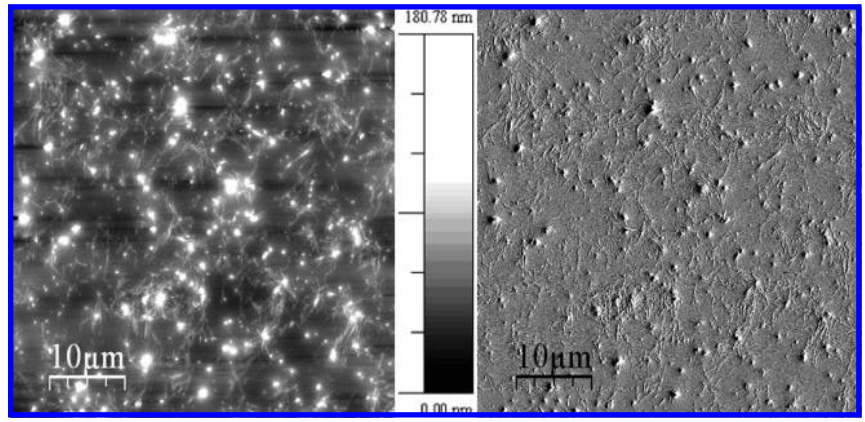

Figure 3. AFM intermittent mode images of QTF12-1.0%DWCNT thin layer on glass substrate. (a) Topography; (b) phase contrast. The images size is 50 μm × 50 μm.

devices, such as the positions of the LUMO and HOMO levels and the width of the band gap, can be determined from appropriately designed electrochemical experiments for example by cyclic voltametry. In order to determine the position of the LUMO and the HOMO levels of the investigated oligomers from the electrochemical data, it is necessary to recalculate their reduction and oxidation potential using the absolute physical potential scale.[21] Assuming that the absolute potential of the Fc/Fc^+ redox couple, that is, the potential referred to the vacuum level, is equal to 4.8 V, the LUMO and the HOMO levels can be calculated as follows[22]

$$E_{LUMO} = -e(E_{ref} + 4.8); \quad E_{HOMO} = -e(E_{ox} + 4.8)$$

The exact determination of the oxidative doping onset potential of an electroactive oligomer (polymer) in a molecular composite with CNTs, by cyclic voltammetry, is usually difficult because its redox peaks are superimposed on an increasing capacitive background originating from the presence of nanotubes.[23] However, the onset potential of this process can more properly be determined from spectroelectrochemical investigations by recording the spectra in a quasi-static mode using stepwise change of the working electrode potential in small increments.[24] After each potential raise, a wait time is applied until the potential change induced current becomes negligible which ensures that the spectra are taken at the equilibrium state. Moreover, this quasi-static mode efficiently eliminates the kinetic effects which may also perturb the precise determination of the HOMO (LUMO) levels by cyclic voltammetry.

Figure 4a shows the evolution of the spectra with increasing electrode potential, recorded for a thin layer of QTF12 deposited on an ITO electrode. The corresponding spectra registered for a thin layer of QTF12-1.0%DWCNT composite are shown in Figure 4b. At the open circuit potential ($E_{oc} = -0.29$ V vs Ag/Ag^+) the oligomer is in its reduced (neutral) state that is characterized by an asymmetric peak at 438 nm with a clear shoulder on its lower energy side. We attribute the dominant peak to the $\pi-\pi^*$ transition in the quaterthiophene subunit whereas the shoulder to the fluorenone moiety. The spectroelectrochemical behavior of QTF12 is classical and resembles that of alternate bithiophene-fluorenone copolymer (PDOBFT) described in ref 25. It starts by the oxidation of the quaterthiophene segment that is spectroscopically manifested by bleaching of the band corresponding to the $\pi-\pi^*$ transition with concomitant growths of two bands at higher wavelengths, originating from the formation of radical cations (polarons) and/or dications (bipolarons).

The presence of these bands is indicative of the oxidative doping. Note that upon increasing electrode potential, the first doping induced band at lower wavelengths undergoes a bathochromic shift whereas that at a higher wavelength it undergoes a hyspochromic one. For the fully doped oligomer (at $E = 0.80$ V vs Ag/Ag^+), the doping induced bands have their maxima at 618 and 1123 nm, respectively, that is, at lower wavelengths (higher energies) that the corresponding bands in oligothiophene-fluorenone copolymer of similar chemical constitution which is consistent with its larger gap.[25] It should also be noted that the fluorenone chromophore band initially present as a shoulder, starts to appear as a separate peak at 464 nm upon the oligothiophene $\pi-\pi^*$ band bleaching and then it is also bleached at higher electrode potentials. On the basis of the spectroelectrochemical data, the onset of the QTF12 oxidative doping, corresponding to the HOMO level, can be estimated as $E = 0.500$ versus Ag/Ag^+.

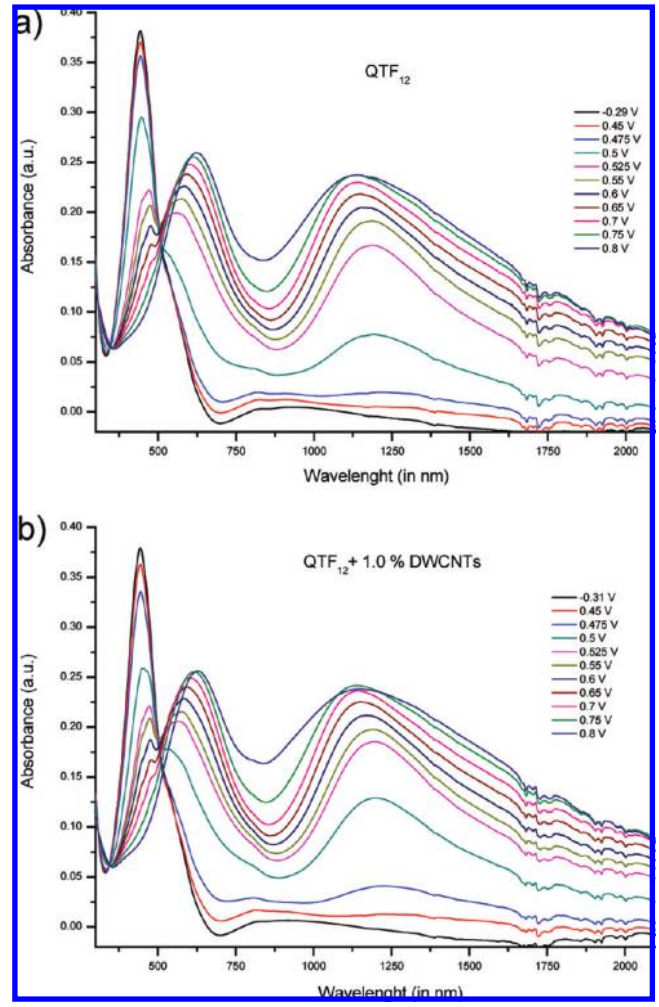

Figure 4. UV−vis-NIR spectra recorded for increasing working electrode potential (electrolyte Bu_4NBF_4/acetonotrile; reference electrode Ag/Ag^+). (a) Thin layer of QTF12 deposited on an ITO electrode, (b) thin layer of QTF12-1.0%DWCNT deposited on an ITO electrode.

The spectra of QTF12-1.0%DWCNT look very similar and are dominated by the bands originating form the oligomer (Figure 4b). It is evident that the oxidation of QTF12 is facilitated by the presence of carbon nanotubes since in the case of the composite the oxidation starts at $E = 0.475$ V versus Ag/Ag^+.

Raman Spectroelectrochemistry. To explore this problem more in detail, we have decided to carry out Raman spectroelectrochemical investigations of QTF12 and its composites with DWCNT. The use of the infrared excitation line ($\lambda_{exc} = 1064$ nm) is especially useful in this case. Because of resonance conditions with the oxidized (doped) form of the oligomer, even minute amounts of doped QTF12 can be detected in the Raman spectra obtained with $\lambda_{exc} = 1064$ nm. In Figure 5a, Raman spectra of QTF12, recorded for increasing electrode potential, are collected.

At the open circuit potential ($E = -0.29$ V versus reference) QTF12 is in its neutral (undoped) state. Two diagnostic bands of the quarterthiophene subunits can be distinguished, a very strong peak at 1454 cm^{-1} and a much weaker one at 1506 cm^{-1}, corresponding $C_\alpha-C_\beta$ symmetric and asymmetric stretchings in the thiophene ring, respectively.[26] The presence of fluorenone gives rise to two peaks, one at 1602 cm^{-1} (C−C stretchings in the aromatic ring) and one at 1720 cm^{-1} (C═O stretchings),

the latter being very weak.[25] The oxidative doping induced spectral changes start to appear at $E = 0.525$ V versus Ag/Ag^+ and are manifested by a bathochromic shift of three bands ($C_\alpha-C_\beta$ stretchings in thiophene and C−C stretchings in the aromatic ring) bands. The C═O stretching band quickly disappears. Concomitantly two new bands at 1225 and 1365 cm^{-1} appear and grow in intensity with increasing electrode potential. These bands are attributed to interring $C_\alpha-C_\alpha$ and intraring $C_\beta-C_\beta$ stretching in the quaterthiophene segments and are indicative of the doping induced quinoid structure formation.[25]

Figure 5b shows the evolution of the Raman spectra of QTF12-1.0%DWCNT imposed by increasing electrode potential. At the open circuit potential ($E_{oc} = -0.31$ V) Raman bands of DWCNT dominate the spectrum despite the fact that they constitute only 1 wt % of the composite. This is an obvious consequence of the resonance enhancement. Close inspection of the DWCNT bands shows that for the infrared excitation line the semiconducting nanotubes are in resonance. The G band at 1589 cm^{-1} is, in this case, Lorentzian in shape; it is accompanied by the G′ band at 2549 cm^{-1} and the D band at 1286 cm^{-1}. From the position of the RBMs modes at 266 and 332 cm^{-1} it can be concluded that the nanotubes being in resonance are of small diameter, 0.9 and 0.7 nm, respectively. The band due to $C_\alpha-C_\beta$ symmetric stretching in QTF12 is clearly seen at 1452 cm^{-1}; however, the band originating from C−C stretchings in the fluorenone moiety is totally obscured by the dominant G band of DWCNT and is seen only as a small shoulder.

The intensity of all DWCNT modes (RBM, D, G, G′) decrease with increasing potential, which means that upon charging the resonance conditions worsen. This is consistent with the previous results reported for pure DWCNT[5b] and their composites with poly(ethylenedioxythiophene).[5c]

As clearly seen from the Raman data, QTF12 molecule, in QTF12-1.0%DWCNT blend, starts to oxidize at $E = 0.450$ V versus Ag/Ag^+. In doped QTF12, the $C_\alpha-C_\beta$ symmetric stretching mode is located at 1434 cm^{-1}, that is, it is bathochromically shifted by 19 cm^{-1} with respect to the corresponding mode in the undoped (neutral) oligomer. Note also that after total disappearance of DWCNT modes at the highest potential, a clear peak at 1589 cm^{-1} can be seen. This is not the G mode of nanotubes but the C−C stretching mode in the aromatic ring of the fluorenone moiety. The C−C mode at 1602 cm^{-1} in neutral QTF12 is shifted to 1589 cm^{-1} in the doped oligomer and fully coincides with the G mode of DWCNT. The potential of the oxidation onset is by 75 mV lower as compared to the corresponding potential in pure QTF12. Similarly as in the case of pure QTF12 two new modes appear upon doping of the oligomer in the composite: 1365 cm^{-1} ($C_\beta-C_\beta$ stretching) and 1225 cm^{-1} ($C_\alpha-C_\alpha$ interring stretching).

It should also be noted that even a very small admixture of DWCNT facilitates the oxidation of the oligomer in the composite, as can be seen in the case of QTF12-0.1%DWCNT whose doping starts at $E = 0.475$ V versus Ag/Ag^+ (Figure 5c).

Both UV−vis-NIR and Raman spectroelectrochemical data consistently show that in the presence of DWCNT the oxidation of QTF12 occurs at a lower potential. This phenomenon cannot be attributed to kinetic facilitation of the oxidative doping process in the presence of electronically conducting DWCNTs because the spectroelectrochemical data were recorded in the equilibrium state (vide supra) Therefore, it must be postulated that the oligomer molecules at the interface with DWCNT

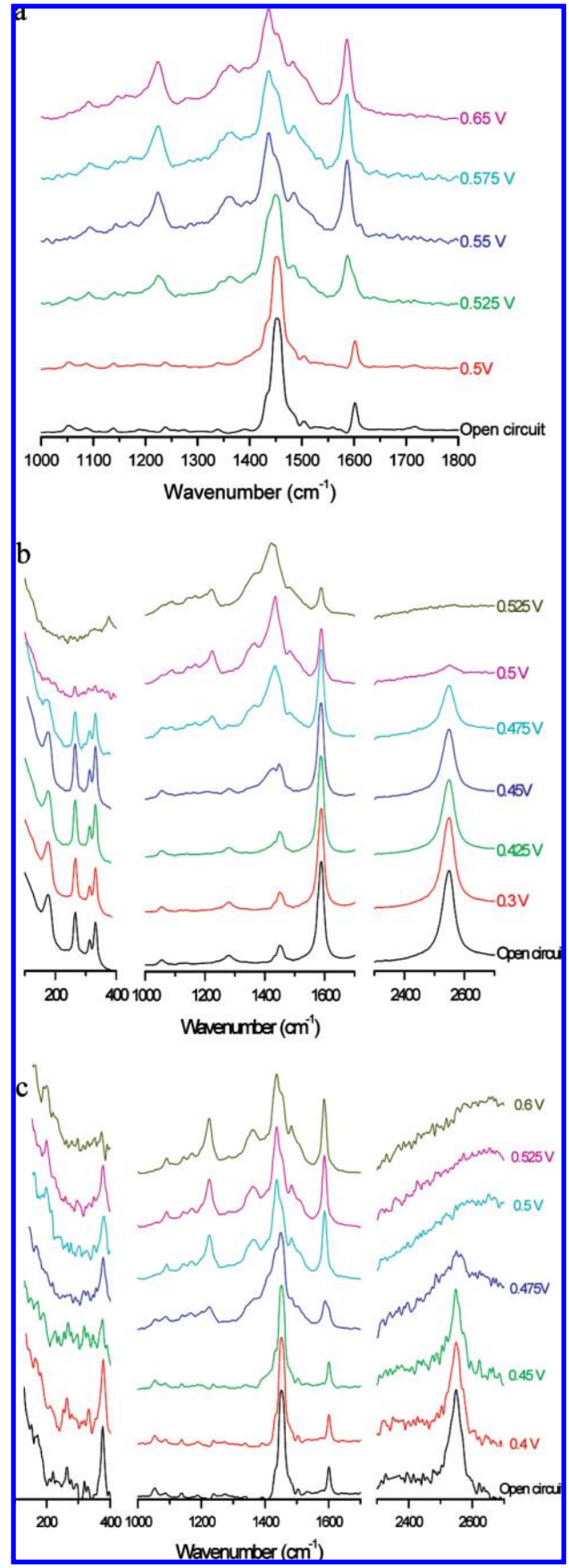

Figure 5. Raman spectra recorded for increasing working electrode potentials ($\lambda_{exc} = 1064$ nm; electrolyte Bu_4NBF_4/acetonotrile; reference electrode Ag/Ag^+). (a) Thin layer of QTF12 deposited on platinum electrode; (b) thin layer of QTF12-1.0%DWCNT deposited on platinum electrode; (c) thin layer of QTF12-0.1%DWCNT deposited on platinum electrode.

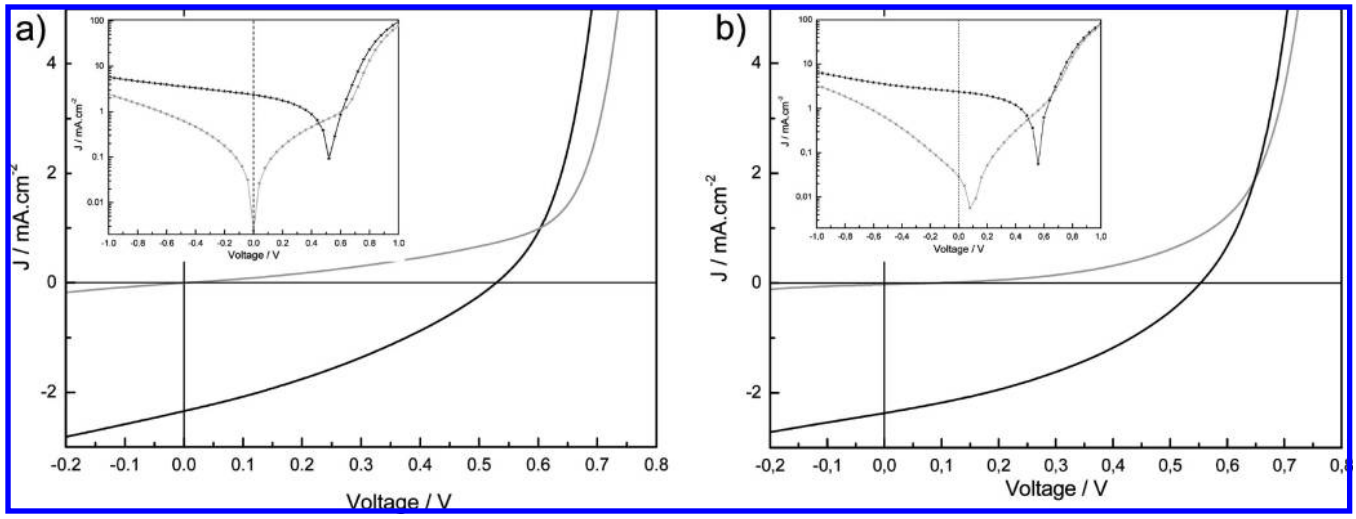

Figure 6. *I*−*V* characteristics of bulk heterojunction solar cells after annealing 5 min at 70 °C in the dark (light gray curve) and illuminated (black curve). (a) PCBM:QTF12-0.1%DWCNT (1:1, PCBM:QTF12 in weight); (b) PCBM:QTF12 (1:1, PCBM:QTF12 in weight).

strongly interact with the nanotubes. As a consequence of these interactions, their HOMO level is raised and they become easier to oxidize.

Photovoltaic Properties. Taking into account their high aspect ratio purely semiconducting nanotubes could be very good candidates as acceptors in bulk heterojunction solar cells with organic donors under the condition that the donor and acceptor energy levels are properly aligned.[2c,3] Carbon nanotubes containing both semiconducting and metallic tubes can also be used as an admixture in conjugated polymer (oligomer), PCBM systems improving charge transport by creating a better pathway.[2g,27] In this research, we have studied such three-component bulk heterojunction cells consisting of PCBM and QTF12-0.1%DWCNT. Figure 6 shows typical *I*−*V* characteristics of the cells.

In the first step we have tested different QTF12/PCBM ratios with no DWCNT present in the junction and we have investigated different thermal treatments of the devices with the goal to optimize these parameters. These parameters were kept identical for fabrication of the devices employing the ternary system as the active layer. The best performances for the QTF12/PCBM based device were obtained for the 1:1 ratio after thermal annealing of the complete cell during 5 min at 70 °C. After annealing, the device showed moderate short circuit current density and V_{oc} values (2.37 mA/cm^2 and 0.56 V); the fill factor value of 0.37 led to a power conversion efficiency of 0.50%.

First, it should be noted that the open circuit voltage value of the cell with DWCNT admixture (V_{oc} = 0.53 V) is by 30 mV lower than the V_{oc} value of the cell without nanotubes, prepared in identical experimental conditions. It is postulated that the V_{oc} value is governed by the energy difference between the HOMO level of the donor and the LUMO level of the acceptor.[28] Thus, this difference may reflect the raise of the HOMO level in QTF12 molecules at the interface, induced by their interactions with DWCNT. This is consistent with the spectroelectrochemical data (vide supra). However, V_{oc} values are also governed by other parameters which are not of thermodynamic nature but which may induce potential losses (resistance of the active layer which is related to its thickness and morphology, carrier recombination, etc.). Therefore, for the majority of bulk heterojunction cells much lower V_{oc} values are usually obtained than theoretically expected ones.[28] Before annealing the device shows moderate short circuit current density (2.11 mA/cm^2) and a rather low fill factor value of 0.31. This indicates that the performance may be limited by charge carrier's recombination. Annealing of the complete device leads to a small drop in V_{oc} with simultaneous small increase in FF, J_{sc} (0.33 and 2.45 mA/cm^2) and the cell efficiency (0.34% before annealing and 0.43% after annealing). These preliminary measurements indicate that the concept of heterojunction of three components is adequate although we observed that DWCNTs have a small detrimental effect on the V_{oc} and the efficiency of the solar cells. However, improvement could be achieved by the optimization of the composition, the thickness, and the morphology of the composites. Further optimization investigations of the devices containing such ternary composites are in progress.

Conclusions

To summarize, we have studied a new composite consisting of 2,7-bis-(3,3‴-didodecyl-[2,2′,5′,2″;5″,2‴]quaterthiophen-5-yl)-fluoren-9-one (QTF12) and double-walled carbon nanotubes (DWCNT) with the aim to study its redox properties and to use it, together with PCBM, for the fabrication of three component bulk heterojunction in organic solar cells. UV−vis-NIR and Raman spectroelectrochemical investigations of this composite unequivocally show that the presence of nanotubes facilitates the oxidation of QTF12, probably via raising the HOMO level of QTF12 molecules being at the interface. Its utility as a component of a bulk heterojunction was proven by the fabrication of solar cells showing an efficiency of 0.43%.

Acknowledgment. The authors thank ANR for funding through the CONAPOSOL research program. Dr. Solenn Berson and Séverine Bailly are acknowledged for their assistance during the fabrication of solar cells. Professor Bernard Ratier and Professor André Moliton are acknowledged for helpful discussions. One of the authors (M.Z.) wants to acknowledge the financial support from Warsaw University of Technology.

Supporting Information Available: Synthesis of QTF12. This material is available free of charge via the Internet at http://pubs.acs.org.

References and Notes

(1) (a) *Handbook of Organic Conductive Molecules and Polymers*; Nalwa H. S., Ed.; John Wiley & Sons Ltd.: Chichester, England, 1997;

Vol. 1−4. (b) *Handbook of Conducting Polymers*; Skotheim, T. A., Elsenbaumer R. L., Reynolds J. R., Eds.; Marcel Dekker, Inc.: New York, 1998; Vol. 1, 2. (c) *Semiconducting Polymers*; Hadziioannou G., Hutten, P. F. V., Eds.; WILEY-VCH: Weinheim, 2007.

(2) (a) Bhattacharyya, S.; Kymakis, E.; Amaratunga, G. A. J. *Chem. Mater.* **2004**, *16*, 4819–4823. (b) Wang, C.; Guo, Z.-X.; Fu, S.; Wu, W.; Zhu, D. *Prog. Polym. Sci.* **2004**, *29*, 1079–1141. (c) Kymakis, E.; Alexandrou, I.; Amaratunga, G. A; J, *J. Appl. Phys.* **2003**, *93* (3), 1764–1768. (d) Ago, H.; Petritsch, K.; Shaffer, M. S. P.; Windle, A. H.; Friend, R. H. *Adv. Mater.* **1999**, *11* (15), 1281–1285. (e) Abdula, D.; Shim, M. *ACS Nano* **2008**, *2*, 2154–2159. (f) Hatton, R. A.; Miller, A. J.; Silva, S. R. P. *J. Mater. Chem.* **2008**, *18*, 1183–1192. (g) Berson, S.; De Bettignies, R.; Bailly, S.; Guillerez, S.; Jousselme, B. *Adv. Funct. Mater.* **2007**, *17*, 3363–3370.

(3) Sgobba, V.; Guldi, D. M. *J. Mater. Chem.* **2008**, *18*, 153–157.

(4) (a) Cheng, F.; Imin, P.; Maunders, C.; Botton, G.; Adronov, A. *Macromolecules* **2008**, *41*, 2304–2308. (b) Kang, Y. K.; Lee, O.; Deria, P.; Kim, S. H.; Park, T.; Bonnell, D. A.; Saven, J. G.; Therien, M. J. *Nano Lett.* **2009**, *9*, 1414–1418. (c) Ikeda, A.; Nobusawa, K.; Hamano, T.; Kikuchi, J. *Org. Lett.* **2006**, *8*, 5489–5492. (d) Rice, N. A.; Soper, K.; Merschrod, E.; Zhao, Y. *Chem. Commun.* **2006**, 4937–4939. (e) Tang, B. Z.; Xu, H. Y. *Macromolecules* **1999**, *32*, 2569–2576. (f) Cheng, F.; Adronov, A. *Chem.—Eur. J.* **2006**, *12*, 5053–5059. (g) Chen, J.; Liu, H. Y.; Weimer, W. A.; Halls, M. D.; Waldeck, D. H.; Walker, G. C. *J. Am Chem. Soc.*; **2002**, *124*, 9034–9035. (h) Curran, S. A.; Ajayan, P. M.; Blau, W. J.; Carroll, D. L.; Coleman, J. N.; Dalton, A. B.; Davey, A. P.; Drury, A.; McCarthy, B.; Maier, S.; Strevens, A. *Adv. Mater.* **1998**, *10*, 1091–1093. (i) Cheng, F.; Adronov, A. *J. Porphyrins Phthalocyanines* **2007**, *11*, 198–204. (j) Cheng, F.; Zhang, S.; Adronov, A.; Echegoyen, L.; Diederich, F. *Chem.—Eur. J.* **2006**, *12*, 6062–6070.

(5) (a) Kalbáč, M.; Kavan, L.; Zukalová, M.; Dunsch, L. *Adv. Funct. Mater.* **2005**, *15*, 418–426. (b) Ladislav, K.; Dunsch, L. *Chem. Phys. Chem.* **2007**, *8*, 974–998. (c) Kalbáč, M.; Kavan, L.; Dunsch, L. *Compos. Sci. Technol.* **2008**, *69*, 1553–1557. (d) Kalbáč, M.; Kavan, L.; Dunsch, L.; Dresselhaus, M. S. *Nano. Lett.* **2008**, *8*, 1257–1264. (e) Zukalová, M.; Tarábek, J.; Kalbáč, M.; Kavan, L.; Dunsch, L. *J. Solid State Electrochem.* **2008**, *12*, 1279–1284.

(6) (a) Tamayo, A. B.; Walker, B.; Nguyen, T. *J. Phys. Chem. C* **2008**, *112*, 11545–11551. (b) Roquet, S.; Cravino, A.; Leriche, P.; Aleveque, O.; Frere, P.; Roncali, J. *J. Am. Chem. Soc.* **2006**, *128*, 3459–3466. (c) Lloyd, M. T.; Mayer, A. C.; Subramanian, S.; Mourey, D. A.; Herman, D. J.; Bapat, A. V.; Anthony, J. E.; Malliaras, G. G. *J. Am. Chem. Soc.* **2007**, *129*, 9144–9149. (d) Kopidakis, N.; Mitchell, W. J.; van de Lagemaat, J.; Ginley, D. S.; Rumbles, G.; Shaheen, S. E.; Rance, W. L. *Appl. Phys. Lett.* **2006**, *89*, 103524–103523.

(7) Lincker, F.; Delbosc, N.; Bailly, S.; De Bettignies, R.; Billon, M.; Pron, A.; Demadrille, R. *Adv. Funct. Mater.* **2008**, *18*, 3444–3453.

(8) Lloyd, M. T.; Anthony, J. E.; Malliaras, G. G. *Mater. Today* **2007**, *10*, 34–41.

(9) Demadrille, R.; Firon, M.; Leroy, J.; Rannou, P.; Pron, A. *Adv. Funct. Mater.* **2005**, *15*, 1547–1552.

(10) Linares, M.; Scifo, L.; Demadrille, R.; Brocorens, P.; Beljonne, D.; Lazzaroni, R.; Grevin, B. *J. Phys. Chem. C* **2008**, *112*, 6850–6859.

(11) Horcas, I.; Fernandez, R.; Gomez-Rodriguez, J. M.; Colchero, J.; Gomez-Herrero, J.; Baro, A. M. *Rev. Sci. Instrum.* **2007**, *78*, 013705.

(12) Demadrille, R.; Delbosc, N.; Kervella, Y.; Firon, M.; De Bettignies, R.; Billon, M.; Rannou, P.; Pron, A. *J. Mater. Chem.* **2007**, *17*, 4661–4669.

(13) Flahaut, E.; Bacsa, R.; Peigney, A.; Laurent, Ch. *Chem. Commun.* **2003**, 1442–1443.

(14) Flahaut, E.; Peigney, A.; Laurent, Ch.; Rousset, A. *J. Mater. Chem.* **2000**, *10*, 249–252.

(15) Kataura, H.; Kumazawa, Y.; Maniwa, Y.; Umezu, I.; Suzuki, S.; Ohtsuka, Y.; Achiba, Y. *Synth. Met.* **1999**, *103*, 2555–2558.

(16) Rao, A. M.; Richter, E.; Bandow, S.; Chase, B.; Eklund, P. C.; Williams, K. A.; Fang, S.; Subbaswamy, K. R.; Menon, M.; Thess, A.; Smalley, R. E.; Dresselhaus, G.; Dresselhaus, M. S. *Science* **1997**, *275*, 187–191.

(17) Piscanec, S.; Lazzeri, M.; Robertson, J.; Chase, B.; Ferrari, A. C.; Mauri, F. *Phys. Rev. B* **2007**, *75*, 035427.

(18) Alvarez, L.; Righi, A.; Guillard, T.; Rols, S.; Anglaret, E.; Laplaze, D.; Sauvajol, J.-L. *Chem. Phys. Lett.* **2000**, *316*, 186–190.

(19) Kuzmany, H.; Planck, W.; Pfeiffer, R.; Simon, F. *J. Raman Spectrosc.* **2008**, *39*, 134.

(20) Herrema, J.; Wildeman, J.; van Bolhuis, F.; Hadziioannou, G. *Synth. Met.* **1993**, *60*, 239–248.

(21) Trassati, S. *Pure Appl. Chem.* **1986**, *58*, 955–966.

(22) Jones, B. A.; Facchetti, A.; Wasielewski, M. R.; Marks, T. J. *J. Am. Chem. Soc.* **2007**, *129*, 15259–15278.

(23) Pokrop, R.; Kulszewicz-Bajer, I.; Wielgus, I.; Zagorska, M.; Albertini, D.; Lefrant, S.; Louarn, G.; Pron, A. *Synth. Met.* **2009**, *159*, 919–924.

(24) Cravino, A.; Neugebauer, H.; Luzzati, S.; Catellani, M.; Petr, A.; Dunsch, L.; Sariciftci, N. S. *J. Phys. Chem. B* **2002**, *106*, 3583–3591.

(25) Demadrille, R.; Divisia-Blohorn, B.; Zagorska, M; Quillard, S.; Rannou, P.; Travers, J. P.; Pron, A. *New J. Chem.* **2003**, *27*, 1479–1484.

(26) Louarn, G.; Trznadel, M.; Buisson, J. P.; Laska, J.; Pron, A.; Lapkowski, M.; Lefrant, S. *J. Phys. Chem.* **1996**, *100*, 12532–12539.

(27) (a) Kymakis, E.; Kornilios, N.; Koudoumas, E. *J. Phys. D: Appl. Phys.* **2008**, *41*, 165110. (b) Arranz-Andrés, J.; Blau, W. J. *Carbon* **2008**, *46*, 2067–2075. (c) Wu, M.; Lin, Y.; Chen, S.; Liao, H.; Wu, Y.; Chen, C.; Chen, Y.; Su, W. *Chem. Phys. Lett.* **2009**, *468*, 64–68.

(28) Cravino, A. *Appl. Phys. Lett.* **2007**, *91*, 243502–243503.

JP906112P